

**Histone H3K9 acetyltransferase PCAF is essential for osteogenic differentiation
through BMP signaling and may be involved in osteoporosis**

Ping Zhang^a, Yunsong Liu^a, Chanyuan Jin^a, Min Zhang^a, Longwei Lv^a, Xiao Zhang^a,
Hao Liu^a, Yongsheng Zhou^{a,b,*}

a Department of Prosthodontics, Peking University School and Hospital of
Stomatology, Beijing 100081, China

b National Engineering Lab for Digital and Material Technology of Stomatology,
Peking University School and Hospital of Stomatology, Beijing 100081, China

* Corresponding author: Yongsheng Zhou, Department of Prosthodontics, Peking
University School and Hospital of Stomatology, 22 Zhongguancun South Avenue,
Haidian District, Beijing100081, China.

Tel.:+86 10 82195370; fax: +86 10 62173402.

E-mail address: kqzhouysh@hsc.pku.edu.cn

Running title: PCAF promotes osteogenic differentiation

Key words: P300/CBP-associated factor, H3K9 acetylation, osteogenic differentiation,
bone morphogenetic protein, osteoporosis

Abstract

Human mesenchymal stem cells (MSCs) are multipotent progenitor cells that can differentiate into osteoblasts, chondrocytes, and adipocytes. The importance of epigenetic regulation for osteogenic differentiation of mesenchymal stem cells (MSCs) is widely accepted. However, the molecular mechanisms are poorly understood. Here we show that histone H3K9 acetyltransferase PCAF plays a critical role in osteogenic differentiation of MSCs. Knockdown of PCAF significantly reduced the bone formation both *in vitro* and *in vivo*. Mechanistically, PCAF controls BMP signaling genes expression by increasing H3K9 acetylation. Most importantly, PCAF expression was significantly decreased in bone sections of ovariectomized or aged mice. Histone modification enzyme is chemically modifiable; therefore, PCAF may represent a novel therapeutic target for stem cell-mediated regenerative medicine and the treatment of osteoporosis.

Introduction

Human mesenchymal stem cells (MSCs) are multipotent progenitor cells with self-renewal capabilities and multilineage differentiation potentials including osteogenesis, chondrogenesis, and adipogenesis [1-4]. Under certain conditions, MSCs are able to differentiate into osteoblasts and hold significant promise for clinical applications, especially for bone regeneration in skeletal defects, largely due to easy harvest, accessibility and lack of immunogenicity [5, 6]. The therapeutic utility of MSCs hinges upon the understanding of molecular mechanisms that regulate

their differentiation [7, 8]. Previous studies have been focused on endeavoring to promote osteogenic differentiation via epigenetic modifications, such as DNA methylation, histone acetylation, and histone methylation [9-11]. Since histone modifications play crucial roles in the osteogenic differentiation, it is of great interest and importance to investigate the individual histone modification enzyme during this process, which may advance our understanding of stem cell fate decision and facilitate the clinical translation of MSCs-mediated bone repair.

Bone homeostasis relies on the inverse relation between adipogenesis and osteogenesis in MSCs. Among a variety of signaling and transcription factors involved in osteogenesis, bone morphogenetic protein (BMP) signaling is a central pathway that controls osteogenic differentiation and bone formation. Knockout experiments showed that a critical threshold level of BMP2 and BMP4 signaling is required for differentiation to mature osteoblasts, and this process is mediated by controlling the transition from $RUNX2^+$ to $RUNX2^+ OSX^+$ cells [12]. Moreover, mouse genetic studies of BMP receptors have revealed important roles for BMP signaling in controlling bone mass [13, 14]. The expression of constitutively active $BMPR1A$ induced adipogenic differentiation, while constitutive BMP receptor 1B ($BMPR1B$) activation induced osteogenic differentiation [15]. Even though BMPs are key regulators of osteogenesis, the precise determinants that govern BMP signaling are poorly understood. More recently, stimulatory effects of BMP2 on osteoblastic differentiation have been reported. The phosphorylation of c-AMP response element

binding protein (CREB) recruits its coactivator CBP (CREB-binding protein) to the promoter of BMP2, thereby promoting BMP2 transactivation [16]. In addition, histone demethylase KDM6B promotes osteogenic differentiation of human MSCs by removing H3K27 me3 on the promoter regions of BMP2 and BMP4 [17]. It is predicted that factors influencing BMP signaling are potential targets for osteogenic regulation.

In the present study, we found that the expression of histone acetyltransferase PCAF was significantly increased after osteogenic induction through Smad signaling. The knockdown of PCAF impaired osteogenic commitment of MSCs both *in vitro* and *in vivo*. Mechanistically, PCAF was required for the expression of BMP pathway genes by increasing histone H3K9 acetylation. Notably, we found that PCAF marks was significantly decreased in bone sections of ovariectomized mice or aged mice. These data suggested that therapies targeting PCAF might suppress the chronic metabolic bone disease commonly found in aged people or menopausal women.

Material and methods

Cell Culture and Osteogenic Induction

Primary human adipose-derived stem cells and bone marrow MSCs were purchased from ScienCell Research Laboratories (Carlsbad, CA, USA). To induce differentiation, MSCs were cultured in osteogenic media containing 100 mM/ml ascorbic acid, 2 mM β -glycerophosphate and 10 nM dexamethasone. All experiments were repeated three

times using human MSCs from the three donors, respectively.

Retroviral infection and Plasmid Constructions

For viral infection, HEK293T cells at 80% confluency were co-transfected with pLNB vectors with a mutant CBA promoter for gene expression or for shRNAs expressions, and with plasmids psPAX2 (Abcam, Cambridge, UK) and pVSV-G (Clontech, USA) using the PolyJet™ Transfection Reagent (SigmaGen Laboratories, Rockville, MD, USA), according to the manufacturer's instructions. The cell culture supernatant was collected at 36, 48 and 60 h after transfection, centrifuged and filtered through a 0.45µm PVDF membrane (Pall Corporation, Port Washington, NY, USA) to remove cellular debris. The viral particles were then precipitated by centrifugation with PEG-it™ (System Biosciences, SBI, Mountain View, CA, USA). The concentrated lentiviral particles were titered, aliquoted and stored at -70°C until ready for use.

In order to facilitate tracking of the knockdown efficiency, we generated lentiviral plasmids for co-expression of red fluorescent protein (RFP) with the target shRNA. We constructed PCAF, SMAD1, and SMAD4 shRNA plasmid with a lentivirus vector expressing RFP.

The target sequences for the shRNA were: *SMAD1sh*, 5'-CTTTCCAGATGCCAGCTGAT-3'; *SMAD4sh*, 5'-CGAGTTGTATCACCTGGAATT-3'; *PCAFsh1*,

5'-GCAGATACCAAACAAGTTTAT-3'; *PCAFsh2*,
5'-GCAGACTTACAGCGAGTCTTT-3'.

For gene overexpression, the Flag-PCAF and Flag-PCAF (deletion 579–608) were cloned into the pLNB vector with a mutant CBA promoter and the lentiviral viruses were packaged as above.

Alkaline phosphatase (ALP) Staining and Quantification

Cells were seeded in six-well plates, and ALP activity was determined by staining with nitroblue tetrazolium and 5-bromo-4-chloro-3-indolyl phosphate on the 7th day after osteogenic differentiation. For quantification of ALP activity, cells were rinsed twice with phosphate-buffered saline (PBS), trypsinized, and then scraped into ddH₂O. This was followed by three cycles of freezing and thawing. ALP activity was determined at 405 nm using p-nitrophenyl phosphate (pNPP) as the substrate. A 50µl sample was mixed with 50µl of pNPP (1 mg/ml) in 1 M diethanolamine buffer containing 0.5 mM MgCl₂ (pH 9.8) and incubated at 37°C for 15 minutes on a bench shaker. The reaction was stopped by the addition of 25 µl of 3 M NaOH/100 µl of reaction mixture. Enzyme activities were quantified by absorbance measurements at 405 nm. Total protein contents were determined using the bicinchoninic acid method using the Pierce (Thermo Fisher Scientific, Rockford, IL, USA) protein assay kit in aliquots of the same samples. The samples were read at 562 nm and calculated against a series of bovine serum albumin (BSA) standards. ALP levels were normalized to the total protein content at the end of the experiment.

Alizarin Red staining and quantification

Analysis of mineralization was determined by Alizarin Red staining. Cells were first rinsed with Milli-Q water, fixed for 30 min in 70% ethanol at 4°C and then rinsed with Milli-Q water. Calcium deposition was then visualized after incubation with 2% Alizarin Red S pH 4.2. Alizarin Red S was extracted by destaining with hexadecyl pyridinium chloride monohydrate, and mineral accumulation was quantified on a microplate reader at 562 nm.

Western Blotting

Western blotting was performed as described previously [18]. We obtained the primary antibodies from the following sources: monoclonal antibody to H3K9 acetylation (Cell Signaling); monoclonal antibody to H3 (Cell Signaling); monoclonal antibody to PCAF (Cell Signaling); monoclonal antibody to actin (Sigma); and monoclonal antibody to flag (Sigma).

Real-time quantitative PCR (RT-qPCR)

We extracted total RNA using Trizol (Invitrogen). We synthesized 0.5-2µg aliquots of RNAs using random hexamers and reverse transcriptase (Takara). We performed the RT-qPCR reactions using the QuantiTect SYBR Green PCR kit (Qiagen) and Life Multi-color Real-time PCR Detection System. The primer sequences were as follows:

Human *GAPDH*, (F) AAGGAGTAAGACCCCTGGACCA, (R)

GCAACTGTGAGCAGGGGAGATT; *RUNX2*, (forward)
 5'-ACTACCAGCCACCGAGACCA-3', (reverse)
 5'-ACTGCTTGCAGCCTTAAATGACTCT-3'; *BGLAP*, (forward)
 5'-CACCATGAGAGCCCTCACACTC-3', (reverse)
 5'-CCTGCTTGGACACAAAGGCTGC-3'; *SPPI*, (forward)
 5'-CAAACGCCGACCAAGGAAAA-3', (reverse)
 5'-TGCCTAGGAGGC AAAAGCAA-3'; *ALP*, (forward)
 5'-TGTGTGGGGTGAAGGCCAAT-3', (reverse)
 5'-TCGTGGTGGTCACAATGCCC-3'; *BMP2*, (forward)
 5'-GACTGCGGTCTCCTAAAGGTCG-3', (reverse)
 5'-CTGGGGAAGCAGCAACGCTA-3'; *BMP4*, (forward)
 5'-AGGCCGAAAGCTGTTACCCG-3', (reverse)
 5'-TACGGAATGGCTCCATGTTCCC-3'; *BMPRIA*, (forward)
 5'-TTCCCTGGGGTCCGGACTTA-3', (reverse)
 5'-ACGACTCCTCCAAGATGTGGC-3'; *BMPR1B*, (forward)
 5'-AGCCTGCCATAAGTGAGAAGCAAA-3', (reverse)
 5'-GGTGGTGGCATTTACAACGCA-3'; *PCAF*, (forward) 5'
 -AGGTTCCCATGGATCTGAAAACC-3' ; (reverse) 5'
 -AAAGACTCGCTGTAAGTCTGCCA-3' ; *GCN5*, (forward) 5'
 -ATCTGGGCGTCTACCTGGCA-3' ; (reverse) 5'
 -ACAGGAATCTGCCATCCCCAGA-3' ; *Pcaf*, (forward) 5'
 -ACCTCGGTACGAAACCACAA-3' ; (reverse) 5'

-TGAAGACCGAGCGAACGAAT-3' .

Chromatin immunoprecipitation (ChIP) assay

Briefly, 2×10^7 cells were cross-linked with 1% formaldehyde, resuspended in lysis buffer (1% sodium dodecyl sulfate [SDS], 10 mM EDTA, and 50 mM Tris-HCl [pH 8.0]) on ice for 3min and fragmented by sonication in RIPA ChIP buffer (0.5 mM EGTA, 140 mM NaCl, 10 mM Tris-HCl, pH 7.5, 1% TritonX-100, 0.01% SDS, 1 mM EDTA and protease inhibitor). Soluble chromatin was then diluted and subjected to immunoprecipitation with the indicated antibodies [PCAF (abcam), H3K9ac (abcam), H3 (abcam)]. Immune complexes were then precipitated with Protein A/G dynabeads, washed sequentially with RIPA ChIP and TE (50 mM NaCl, 5 mM EDTA, and 50 mM Tris-HCl [pH 8.0]) buffer. After the cross-linking was reversed, immune complexes containing DNA were purified and eluted. The precipitated DNA was subjected to RT-qPCR analysis. Sequences of ChIP primers were as follows: *BMP2*, (forward) 5'-TAGGAGAGCGAGGGGAGAG-3', (reverse) 5'-CTCGCCAGTTGAAAGCACCC-3'; *BMP4*, (forward) 5'-CTCTTTCCCTCCCTCGCTTT-3', (reverse) 5'-GAGGAGGGAAGGAGGGAGG-3'; *RUNX2*, (forward): 5'-GGAGATCATCGCCGACCA-3', (reverse) 5'-CACCGAGCACAGGAAGTTG-3'; *BMPRI1B*, (forward) 5'-TTCTTACATCCGGGTGTGCT-3', (reverse) 5'-GGCACCAGGTTTAACAGCAA-3'.

Bone formation *in vivo*

Nude mouse implantation was performed as described [19]. Briefly, 2×10^6 cells were mixed with Bio-Oss Collagen (Geistlich, Switzerland) and then transplanted subcutaneously into the dorsa of nude mice. Two transplantation sites were prepared in each mouse and transplanted with three groups of cells: MSC/Scrsh, MSC/PCAF sh#1, and MSC/PCAF sh#2. After 6 weeks, transplants were harvested and prepared for histological analysis. All animal work of this study was approved by the Peking University Biomedical Ethics Committee Experimental Animal Ethics Branch. Specimens of each group were harvested at 6 weeks after implantation, and animals in each group were sacrificed by CO₂ asphyxiation. The bone constructs were fixed in 4% paraformaldehyde and then decalcified for 10 days in 10% EDTA (pH 7.4). After decalcification, the specimens were dehydrated and subsequently embedded in paraffin. Sections (5-mm thickness) were stained with hematoxylin and eosin (H&E) and Masson's trichrome stain.

Micro CT analysis of mice

C57BL/6 mice were obtained from The Jackson Laboratory (Bar Harbor, ME, USA). Mice were maintained in a pathogen-free facility on a 12 hour light/dark cycle with water and food provided *ad libitum*. Five-month-old mice were sham-operated (sham) or ovariectomized (OVX). The OVX mice presented osteoporosis as described previously [20]. Mice were allowed 3 months to recover from the ovariectomy

surgery and then sacrificed for the related assays. Osteoporosis is also an age-related marker in mice [21]; therefore, female 2-month-old mice (young) and 16-month-old mice (old) were also studied.

The proximal femur and tibia thoroughly dissected free of soft tissue was fixed with 4% paraformaldehyde for 24h and subsequently washed with 10% sucrose solution. Twelve hours later, images were scanned at a resolution of 8.82 μm , with tube voltage of 80 kV, tube current of 500 μA and exposure time of 1500 ms. A typical examination consisted of a scout view, selection of the examination volume, automatic positioning, measurement, offline reconstruction, and evaluation. Two-dimensional images were used to generate 3D reconstructions using multimodal 3D visualization software (Inveon Research Workplace, Siemens, Munich, Germany) supplied by the micro-CT system.

To evaluate the mass and microarchitecture in bone between different groups, micro-CT was undertaken using an Inveon MM system (Siemens). Images were acquired at an effective pixel size of 8.82 μm , voltage of 80 kV, current of 500 μA and exposure time of 1500 ms in each of the 360 rotational steps. Parameters were calculated using an Inveon Research Workplace (Siemens) as follows: bone volume/total volume (BV/TV), trabecular thickness (Tb.Th), trabecular number (Tb.N), and trabecular separation (Tb.Sp) in the trabecular region (1–2 mm distal to the proximal epiphysis) according to guidelines set by the American Society for Bone and Mineral Research [22].

Histology and immunofluorescence staining of bone sections

Bones were fixed in 4% paraformaldehyde at 4°C under constant agitation for 3 days. Bones were then decalcified in 14% EDTA solution (EDTA dissolved in Milli-Q water, and the pH was adjusted to 7.1 with ammonium hydroxide) at 4°C or RT under constant agitation for 3–5 days (fresh 14% EDTA solution was exchanged every 34 h). Bones were then washed in PBS for 2 h, soaked in 30% sucrose in PBS at 4°C under constant agitation overnight and finally embedded in optimal cutting temperature (OCT) compound. Free-floating sections (30- μ m thick) were processed for immunohistochemistry as described previously [23] with minor modifications. The anti-PCAF antibody (Abcam, 1:100) was applied overnight at 4°C. The secondary antibody used was Alexa Fluor 546 labeled-goat anti-rabbit IgG (Invitrogen, 1:2000). Cell nuclei were counter stained with Hoechst 33358 (Invitrogen). Fluorescence images were acquired with a confocal laser scanning microscope (LSM510; Oberkochen, Germany).

Statistical analysis

All statistical analyses were performed using the GraphPad scientific software for Windows (San Diego, CA). Comparisons between two groups were analyzed by independent two-tailed Student's t-tests, and comparisons between more than two groups were analyzed by one-way ANOVA followed by a Tukey's *post hoc* test. Data were expressed as the mean \pm standard deviation (SD) of 3–10 experiments per group. P values <0.05 were considered statistically significant.

Results

PCAF expression is increased by osteogenic induction through Smad in MSCs

To investigate potential roles of histone H3K9 acetyltransferases in osteogenic differentiation of MSCs, we investigated expressions of PCAF and GCN5 in MSCs after osteogenic induction. As shown in SFig. 1A-B, the extracellular matrix mineralization was significantly increased as determined by Alizarin Red S staining and quantification at 2 weeks after osteogenic induction. Then the total RNA was extracted from both control cells and induced cells. The RT-qPCR revealed that the expression of both *PCAF* and *GCN5* was significantly induced after osteogenic differentiation (SFig. 1C). To better understand the role that PCAF and GCN5 play in the osteogenic differentiation, we further analyzed the endogenous expression profile of *PCAF* and *GCN5* in MSCs after osteogenic differentiation at 0 day, 3 days, 7 days, and 14 days. As shown in Fig. 1A-C, increased expression of *PCAF* and *GCN5* was paralleled by upregulation of osteogenic marker *RUNX2*, as determined by RT-qPCR. A similar pattern was also observed at protein level, as indicated by western blot analysis (Fig. 1D). In addition, BMP2 treatment promoted the *PCAF* expression effectively, but not *GCN5* expression, as shown in SFig. 1D-E. BMP/SMAD signaling is a key regulator for osteogenic differentiation of stem cells, we next examined whether the induction of PCAF was dependent on SMAD signaling. Lentiviruses expressing *SMAD1* shRNA was generated to knockdown *SMAD1*.

Western blot analysis and fluorescent staining showed that SMAD1 was effectively depleted in MSCs expressing *SMAD1* shRNA compared with MSCs expressing scramble shRNA (Fig. 1E & SFig. 1F). As shown in Fig. 1F-G & SFig. 1G, knockdown of *SMAD1* dramatically reduced the expressions of *PCAF*, but not *GCN5* in MSCs cultured in osteogenic media. Furthermore, the knockdown of *SMAD4*, another key factor associated with BMP signaling, also inhibited *PCAF* but not *GCN5* expressions induced by osteogenic induction (Fig. 1H-I & SFig. 1H-I).

PCAF is required for osteogenic differentiation in vitro

Since PCAF expression was increased after osteogenic induction, we next explored whether PCAF play a role in osteogenic differentiation of MSCs. We first established *PCAF* stable knock-down MSCs using lentiviral vectors expressing a short hairpin RNA (shRNA). To rule out off target effects, two shRNA sequences against *PCAF* were designed. The knockdown efficiency was confirmed by fluorescent staining and western blotting (SFig. 2A & Fig. 2A). After culturing the MSCs in osteogenic media for 7 days, ALP activity was detected and found to be significantly suppressed by *PCAF* knockdown (Fig. 2B & C). Since the ALP activity increases and then decreases during the osteogenic differentiation, to be sure that our observation is not due to a shift of the activity curve to longer or shorter times, we examined the ALP activity after culturing the MSCs in osteogenic media for 0 day, 4 days, 7 days, 10 days, 12 days, and 14 days. As shown in SFig. 2B, the ALP activity increased after osteogenic

induction at 7 days, while decreased after 12 days of osteogenic differentiation. Moreover, the extracellular matrix mineralization, as determined by Alizarin Red S staining and quantification, was also impaired in *PCAF* knockdown cells at 2 weeks after osteogenic induction (Fig. 2D & E). To confirm that *PCAF* depletion inhibited osteogenic differentiation, we investigated several osteogenic markers when MSCs were treated with osteogenic induction. As shown in Fig. 2F-H & SFig. 2C, in contrast to the control cells, knockdown of *PCAF* resulted in significantly decreased mRNA expression levels of *SPPI*, *BGLAP*, *ALP*, and *RUNX2*. Taken together, these results indicated that *PCAF* is required for osteogenic differentiation *in vitro*.

The regulation of osteogenic differentiation by *PCAF* is dependent on its HAT activity

In order to further confirm the function of *PCAF* in the osteogenic differentiation process, we next established the *PCAF* rescue cell line with the vector, flag-*PCAF* (wild-type, WT) and flag-*PCAF* mutant (deletion 579–608, lacking the histone acetyltransferase activity) [24] (Fig. 3A & SFig. 3A). As shown in Fig. 3B-C, only WT *PCAF* but not the catalytic mutant *PCAF* could promote the ALP activity in response to osteogenic stimulation. Similarly, when MSCs were treated with differentiation media at 2 weeks, only WT *PCAF* could enhance the formation of mineralization nodules (Fig. 3D-E). Thus, the regulation of osteogenic differentiation by *PCAF* appeared to be dependent on its HAT activity. In addition, we detected the expression of osteogenesis-associated genes in the *PCAF* rescue cell line under

osteogenic induction. These genes were only upregulated in WT PCAF-overexpressing cells compared with the control cells and mutant PCAF-overexpressing cells (Fig. 3F-H & SFig. 3B). Together, these results indicated that the HAT activity of PCAF is indispensable for the regulation of osteogenic differentiation.

PCAF are required for MSC-mediated bone formation in vivo

To verify our *in vitro* findings, we examined whether the knockdown of *PCAF* affected MSC-mediated bone formation *in vivo*. H&E staining showed that *PCAF* knockdown cells formed less bone tissues than control cells (Fig. 4A-B & SFig. 4A). Consistent with the observations from H&E staining, the osteogenic differentiation potential was markedly decreased for hybrids containing PCAF sh/MSCs compared with control cells, as detected by Masson' trichrome staining (Fig. 4C & SFig. 4B). As a whole, these results indicated the novel role of PCAF in bone formation *in vivo*.

Inhibition of adipocyte lineage commitment of MSCs by PCAF

As normal bone homeostasis relies on the balance between osteogenesis and adipogenesis in differentiating MSCs, an osteogenic lineage commitment could be coupled with an inhibition of adipogenic differentiation. To explore the potential role of PCAF in regulating adipogenic differentiation of MSCs, PCAF sh MSCs and control cells were grown in adipogenic-inducing media, after 3 weeks of culture, we performed Oil-Red-O staining to detect the lipid droplets. As shown in Fig. 4D, we

observed increase of adipogenesis in PCAF sh MSCs as compared with control cells. In addition, the depletion of PCAF enhanced the mRNA level of the master adipogenic transcription factor PPAR- γ , as shown in SFig. 4C.

PCAF acetylates histone H3K9 at promoters of BMP pathway genes

In order to explore the molecular mechanisms underlying the regulation of osteogenic differentiation by PCAF, we performed RT-qPCR analysis to assess the expression of key genes associated with osteogenic differentiation of MSCs. As shown in SFig. 5A, *PCAF* knockdown with both shRNAs led to reduction in the expressions of a subset of BMP signaling genes, including *BMP2*, *BMP4*, *SMAD1*, *BMPR1B*, *RUNX2*. However, overexpression of WT PCAF, but not a PCAF mutant caused a significant increase in the indicated genes (SFig. 5B). Based on these data, we extended our investigation to determine whether PCAF associates with promoters of BMP pathway genes, using chromatin immunoprecipitation (ChIP) analysis. Compared with the IgG negative control signals, we detected obvious PCAF occupancy at the indicated promoters (Fig. 5A-D). To further confirm PCAF binding to the indicated gene promoter, we observed that the knockdown of PCAF reduced PCAF binding to the *BMP2*, *BMP4*, *BMPR1B*, and *RUNX2* promoters by ChIP assays (SFig. 5C-F). Consistently, decreased binding of PCAF at the promoter regions was associated with decreased appearance of its substrate, H3K9 ac, which is a hallmark of gene activation (Fig. 5E-H). Collectively, these results suggested that PCAF was recruited to promoters of BMP pathway genes to acetylate H3K9 and activate BMP signaling.

To further determine the functional connection between PCAF and BMP signaling in osteogenic differentiation, we examined the effect of BMP2 on osteogenesis in *PCAF*-knockdown cells. As shown in SFig. 6A-B, treatment of *PCAF* knockdown cells with BMP2, could reverse the ALP activity caused by PCAF deficiency. Moreover, knockdown of *SMAD1* alters PCAF-controlled *RUNX2* expression in MSCs, as shown in SFig. 6C-D. It is well-known that BMP signaling regulates cells function via Smads, collectively, our data suggested that PCAF promotes osteogenic differentiation through the BMP/SMAD signaling pathway.

PCAF is decreased in bone sections of osteoporotic mice

Previously, the ovariectomized (OVX) mice were verified to display significantly increased adipogenesis and decreased osteogenesis in their bone marrow with osteoporosis [25]. To evaluate the possible functional significance of PCAF in bone remodeling *in vivo*, we produced OVX mice as an animal model of postmenopausal osteoporosis. Compared with sham-operated mice, OVX mice exhibited significantly increased adipose tissues and decreased trabecular bones, as shown in Fig. 6A-C & SFig. 7A-B. Next we examined whether PCAF was impaired during osteoporosis, using immunohistochemistry staining. While PCAF in femur bone sections stained very strongly in sham-operated mice, the expressions of PCAF was detected very weakly in OVX mice (Fig. 6D-E). In aged mice, adipogenesis is also increased in bone marrow whereas osteoblastogenesis is reduced [26]. Compared with younger, 2-month-old mice, we observed that adipose tissues were significantly increased in

the bone marrows of 16-month old mice, and micro CT showed that the trabecular bone was significantly reduced in 16-month-old mice compared with the 2-month-old mice (Fig. 6F-H & SFig. 7C-D). To further confirm that PCAF is associated with osteogenic differentiation, we also examined their status in aged mice. In contrast to the 2-month-old mice, immunohistochemistry and confocal microscopy of femur sections in 16-month-old mice showed decreased PCAF staining (Fig. 6I-J).

In addition, we isolated MSCs from sham mice, OVX-ed mice, 2-month-old mice, and 16-month-old mice separately. Mouse MSCs used in our studies are nestin-positive cells (SFig. 7E-F). RT-qPCR revealed that the expression of *Pcaf* was decreased in MSCs from OVX-ed compared with those from sham mice (SFig. 7G). Compared with 2-month-old mice, MSCs from 16-month-old mice also displayed significantly reduced *Pcaf* expression (SFig. 7H).

Discussion

The fate decision and lineage differentiation of MSCs is a complex biological process orchestrated by multiple layers of regulation including epigenetic, transcriptional and post-transcriptional ways. It has becoming increasingly clear that the chromatin modifications play crucial roles during these processes [27]. Modified histone domains have been identified as epigenetic signatures that either mark for gene activation, such as acetylated histone H3K9 and trimethylated histone H3K4, or mark for gene repression, such as trimethylated H3K9 and H3K27 [28, 29]. In the present study, we detected that both H3K9 acetyltransferase GCN5 and PCAF were induced

after osteogenic differentiation. Interestingly, GCN5 was identified to regulate osteogenic commitment of MSCs independent of its HAT activity in our previous study [19]; but the HAT activity of PCAF is indispensable for the regulation of osteogenic differentiation in this work. In addition, we detected that PCAF played a critical role in osteogenic differentiation by increasing H3K9 acetylation on BMP signaling genes. More importantly, given the inverse relationship between osteogenic and adipogenic lineage commitment, we found that PCAF was abnormally decreased in bone sections of osteoporotic mice. Together, our findings highlighted that PCAF-mediated chromatin modification played an important role in the osteogenic differentiation and in the metabolic bone disease.

Recently, accumulating evidence has showed that histone modification enzymes contribute to normal skeletal development and bone formation. For instance, *Sirt6*-deficient mice exhibits low bone mineral density; HDAC2 mutant mice and HDAC3 knockout mice exhibit severe bone defects such as reduced body size resulting from impaired endochondral bone formation [30-32]; Moreover, H3K4me3 demethylase RBP2 was reported to regulate osteogenic differentiation *in vitro* and *in vivo* [33], and histone demethylases KDM4B and KDM6B play critical roles in osteogenic commitment of MSCs by removing H3K9me3 and H3K27me3 [17]. However, little is known about the role of histone acetyltransferase in osteoblast differentiation and bone formation. Here, we provide evidence that PCAF has a stimulative effect on osteogenic differentiation of MSCs. Consistent with our findings,

one early study show that PCAF acetylates Runx2 to promote osteoblast differentiation [34]. The novelty of our work lies in: First, PCAF expression increased during the osteogenic process through Smad signaling. Second, the regulation of osteogenic differentiation by PCAF is dependent on its HAT activity. Third, PCAF regulates osteogenic differentiation by increasing H3K9 acetylation on BMP signaling genes. Additionally, we found that PCAF knockdown significantly impaired bone formation in vivo. Finally, we detected that PCAF expression was decreased in bone sections of osteoporotic mice. Our results revealed the detailed underlying molecular mechanism by which PCAF regulates osteogenic differentiation, on the other hand, we first verified that PCAF might play important roles in the development of osteoporosis by influencing the determination of MSCs' fate. Most importantly, our present work shed light on the function of epigenetic mark H3K9 acetylation and histone acetyltransferase PCAF in the MSCs lineage commitment and metabolic bone disease.

PCAF is a member of the GNAT (GCN5-related N-acetyltransferase) family of protein acetyltransferases [35]. This histone acetyltransferase has roles in regulation of transcription, cell cycle progression, and differentiation [24, 36, 37]. Functional and structural characterization of PCAF acetyltransferase activity indicated that Lysines 9 and 14 of histone H3 are the preferred substrates, and these residues appear to play a critical role in promoting the association of histone H3 with PCAF [38, 39]. There is also increasing evidence that PCAF modulates non-histone proteins [40-43]

including hypoxia-inducible factor 1 α (Hif-1 α) [44] and Notch [45]. In the present study, we generated PCAF wild type and PCAF mutant (deletion 579–608, lacking the histone acetyltransferase activity) rescue cells, only WT PCAF but not the catalytically mutant PCAF is capable of promoting osteogenic differentiation. Our data also show that PCAF positively regulates BMP signaling via histone H3K9 acetylation. These finding supported the role of histone acetyltransferase PCAF in gene expression via modulation of chromatin [46]. In addition to histone acetylation, histone methylation has recently been identified as a key modulator of MSC lineage specification as well [17, 33]. The regulation of MSC lineage specification by SET domain-containing histone lysine methyltransferases (KMTs) and JmjC domain-containing histone lysine demethylases (KDMs) has been well studied [47]. However, whether there is a connection between acetylation and methylation of histone is still vague and whether histone acetylation and methylation may cooperate with each other during the lineage commitment of MSCs needs further investigation.

Osteoporosis is one of the most common bone metabolic diseases and is associated with a shift in MSCs lineage commitment [48, 49]. Our immunostaining analysis revealed decreased PCAF expression in bone sections of osteoporotic mice. These results indicated that PCAF might play important roles in the development of osteoporosis by influencing the determination of MSCs' fate. Histone acetyltransferase is chemically modifiable; therefore, PCAF may have potentials as a therapeutic target for stem cell-mediated regenerative medicine, as well as treatment

of osteoporosis.

Disclosures

The authors indicate no potential conflicts of interest.

Acknowledgments

This study was supported by grants from the National Natural Science Foundation of China (No. 81500822, No. 81570953), the Program for New Century Excellent Talents in University from Ministry of Education (NCET-11-0026), the PKU School of Stomatology for Talented Young Investigators (PKUSS20140109), and the Construction Program for National Key Clinical Specialty from National Health and Family Planning Commission of China (2011).

Reference

- [1] Bianco P, Robey PG, Simmons PJ. Mesenchymal stem cells: revisiting history, concepts, and assays. *Cell stem cell* 2008;2:313-9.
- [2] Caplan AI. Adult mesenchymal stem cells for tissue engineering versus regenerative medicine. *Journal of cellular physiology* 2007;213:341-7.
- [3] Levi B, Longaker MT. Concise review: adipose-derived stromal cells for skeletal regenerative medicine. *Stem cells (Dayton, Ohio)* 2011;29:576-82.
- [4] Teitelbaum SL. Stem cells and osteoporosis therapy. *Cell stem cell* 2010;7:553-4.
- [5] Caplan AI, Bruder SP. Mesenchymal stem cells: building blocks for molecular medicine in the 21st century. *Trends in molecular medicine* 2001;7:259-64.
- [6] Kon E, Filardo G, Roffi A, Di Martino A, Hamdan M, De Pasqual L, et al. Bone regeneration with mesenchymal stem cells. *Clinical cases in mineral and bone metabolism : the official journal of the Italian Society of Osteoporosis, Mineral Metabolism, and Skeletal Diseases* 2012;9:24-7.
- [7] Medici D, Shore EM, Lounev VY, Kaplan FS, Kalluri R, Olsen BR. Conversion of vascular endothelial cells into multipotent stem-like cells. *Nature medicine* 2010;16:1400-6.
- [8] Huebsch N, Arany PR, Mao AS, Shvartsman D, Ali OA, Bencherif SA, et al. Harnessing traction-mediated manipulation of the cell/matrix interface to control stem-cell fate. *Nature materials* 2010;9:518-26.

- [9] Villagra A, Gutierrez J, Paredes R, Sierra J, Puchi M, Imschenetzky M, et al. Reduced CpG methylation is associated with transcriptional activation of the bone-specific rat osteocalcin gene in osteoblasts. *Journal of cellular biochemistry* 2002;85:112-22.
- [10] Lee HW, Suh JH, Kim AY, Lee YS, Park SY, Kim JB. Histone deacetylase 1-mediated histone modification regulates osteoblast differentiation. *Molecular endocrinology (Baltimore, Md)* 2006;20:2432-43.
- [11] Wei Y, Chen YH, Li LY, Lang J, Yeh SP, Shi B, et al. CDK1-dependent phosphorylation of EZH2 suppresses methylation of H3K27 and promotes osteogenic differentiation of human mesenchymal stem cells. *Nature cell biology* 2011;13:87-94.
- [12] Bandyopadhyay A, Tsuji K, Cox K, Harfe BD, Rosen V, Tabin CJ. Genetic analysis of the roles of BMP2, BMP4, and BMP7 in limb patterning and skeletogenesis. *PLoS genetics* 2006;2:e216.
- [13] Kamiya N, Ye L, Kobayashi T, Lucas DJ, Mochida Y, Yamauchi M, et al. Disruption of BMP signaling in osteoblasts through type IA receptor (BMPRIA) increases bone mass. *J Bone Miner Res* 2008;23:2007-17.
- [14] Kamiya N, Kobayashi T, Mochida Y, Yu PB, Yamauchi M, Kronenberg HM, et al. Wnt inhibitors Dkk1 and Sost are downstream targets of BMP signaling through the type IA receptor (BMPRIA) in osteoblasts. *J Bone Miner Res* 2010;25:200-10.
- [15] Chen D, Ji X, Harris MA, Feng JQ, Karsenty G, Celeste AJ, et al. Differential roles for bone morphogenetic protein (BMP) receptor type IB and IA in differentiation and specification of mesenchymal precursor cells to osteoblast and adipocyte lineages. *J Cell Biol* 1998;142:295-305.
- [16] Shim JH, Greenblatt MB, Singh A, Brady N, Hu D, Drapp R, et al. Administration of BMP2/7 in utero partially reverses Rubinstein-Taybi syndrome-like skeletal defects induced by Pdk1 or Cbp mutations in mice. *J Clin Invest* 2012;122:91-106.
- [17] Ye L, Fan Z, Yu B, Chang J, Al Hezaimi K, Zhou X, et al. Histone demethylases KDM4B and KDM6B promotes osteogenic differentiation of human MSCs. *Cell stem cell* 2012;11:50-61.
- [18] Zhang P, Tu B, Wang H, Cao Z, Tang M, Zhang C, et al. Tumor suppressor p53 cooperates with SIRT6 to regulate gluconeogenesis by promoting FoxO1 nuclear exclusion. *Proceedings of the National Academy of Sciences of the United States of America* 2014;111:10684-9.
- [19] Zhang P, Liu Y, Jin C, Zhang M, Tang F, Zhou Y. Histone Acetyltransferase GCN5 Regulates Osteogenic Differentiation of Mesenchymal Stem Cells by Inhibiting NF-kappaB. *Journal of bone and mineral research : the official journal of the American Society for Bone and Mineral Research* 2015.
- [20] Ducy P, Desbois C, Boyce B, Pinero G, Story B, Dunstan C, et al. Increased bone formation in osteocalcin-deficient mice. *Nature* 1996;382:448-52.
- [21] Weiss A, Arbell I, Steinhagen-Thiessen E, Silbermann M. Structural changes in aging bone: osteopenia in the proximal femurs of female mice. *Bone* 1991;12:165-72.
- [22] Bouxsein ML, Boyd SK, Christiansen BA, Guldberg RE, Jepsen KJ, Muller R. Guidelines for assessment of bone microstructure in rodents using micro-computed tomography. *J Bone Miner Res* 2010;25:1468-86.
- [23] Kennedy J, Baris C, Hoyland JA, Selby PL, Freemont AJ, Braidman IP. Immunofluorescent localization of estrogen receptor-alpha in growth plates of rabbits, but not in rats, at sexual maturity. *Bone* 1999;24:9-16.
- [24] Puri PL, Sartorelli V, Yang XJ, Hamamori Y, Ogryzko VV, Howard BH, et al. Differential roles of p300 and PCAF acetyltransferases in muscle differentiation. *Molecular cell* 1997;1:35-45.
- [25] Chang J, Wang Z, Tang E, Fan Z, McCauley L, Franceschi R, et al. Inhibition of osteoblastic bone

- formation by nuclear factor- κ B. *Nature medicine* 2009;15:682-9.
- [26] Muruganandan S, Roman AA, Sinal CJ. Adipocyte differentiation of bone marrow-derived mesenchymal stem cells: cross talk with the osteoblastogenic program. *Cell Mol Life Sci* 2009;66:236-53.
- [27] Teven CM, Liu X, Hu N, Tang N, Kim SH, Huang E, et al. Epigenetic regulation of mesenchymal stem cells: a focus on osteogenic and adipogenic differentiation. *Stem cells international* 2011;2011:201371.
- [28] Shi Y. Histone lysine demethylases: emerging roles in development, physiology and disease. *Nature reviews Genetics* 2007;8:829-33.
- [29] Agger K, Christensen J, Cloos PA, Helin K. The emerging functions of histone demethylases. *Current opinion in genetics & development* 2008;18:159-68.
- [30] Mostoslavsky R, Chua KF, Lombard DB, Pang WW, Fischer MR, Gellon L, et al. Genomic instability and aging-like phenotype in the absence of mammalian SIRT6. *Cell* 2006;124:315-29.
- [31] Razidlo DF, Whitney TJ, Casper ME, McGee-Lawrence ME, Stensgard BA, Li X, et al. Histone deacetylase 3 depletion in osteo/chondroprogenitor cells decreases bone density and increases marrow fat. *PloS one* 2010;5:e11492.
- [32] Zimmermann S, Kiefer F, Prudenziati M, Spiller C, Hansen J, Floss T, et al. Reduced body size and decreased intestinal tumor rates in HDAC2-mutant mice. *Cancer research* 2007;67:9047-54.
- [33] Ge W, Shi L, Zhou Y, Liu Y, Ma GE, Jiang Y, et al. Inhibition of osteogenic differentiation of human adipose-derived stromal cells by retinoblastoma binding protein 2 repression of RUNX2-activated transcription. *Stem cells* 2011;29:1112-25.
- [34] Wang CY, Yang SF, Wang Z, Tan JM, Xing SM, Chen DC, et al. P/CAF acetylates Runx2 and promotes osteoblast differentiation. *Journal of bone and mineral metabolism* 2013;31:381-9.
- [35] Yang XJ, Ogryzko VV, Nishikawa J, Howard BH, Nakatani Y. A p300/CBP-associated factor that competes with the adenoviral oncoprotein E1A. *Nature* 1996;382:319-24.
- [36] Xenaki G, Ontikatzte T, Rajendran R, Stratford IJ, Dive C, Krstic-Demonacos M, et al. P/CAF is an HIF-1 α cofactor that regulates p53 transcriptional activity in hypoxia. *Oncogene* 2008;27:5785-96.
- [37] Zheng X, Gai X, Ding F, Lu Z, Tu K, Yao Y, et al. Histone acetyltransferase P/CAF up-regulated cell apoptosis in hepatocellular carcinoma via acetylating histone H4 and inactivating AKT signaling. *Mol Cancer* 2013;12:96.
- [38] Schiltz RL, Mizzen CA, Vassilev A, Cook RG, Allis CD, Nakatani Y. Overlapping but distinct patterns of histone acetylation by the human coactivators p300 and P/CAF within nucleosomal substrates. *J Biol Chem* 1999;274:1189-92.
- [39] Poux AN, Marmorstein R. Molecular basis for Gcn5/P/CAF histone acetyltransferase selectivity for histone and nonhistone substrates. *Biochemistry* 2003;42:14366-74.
- [40] Imhof A, Yang XJ, Ogryzko VV, Nakatani Y, Wolffe AP, Ge H. Acetylation of general transcription factors by histone acetyltransferases. *Current biology : CB* 1997;7:689-92.
- [41] Liu L, Scolnick DM, Trievel RC, Zhang HB, Marmorstein R, Halazonetis TD, et al. p53 sites acetylated in vitro by P/CAF and p300 are acetylated in vivo in response to DNA damage. *Molecular and cellular biology* 1999;19:1202-9.
- [42] Sartorelli V, Puri PL, Hamamori Y, Ogryzko V, Chung G, Nakatani Y, et al. Acetylation of MyoD directed by P/CAF is necessary for the execution of the muscle program. *Molecular cell* 1999;4:725-34.
- [43] Itoh S, Ericsson J, Nishikawa J, Heldin CH, ten Dijke P. The transcriptional co-activator P/CAF potentiates TGF- β /Smad signaling. *Nucleic acids research* 2000;28:4291-8.

- [44] Lim JH, Lee YM, Chun YS, Chen J, Kim JE, Park JW. Sirtuin 1 modulates cellular responses to hypoxia by deacetylating hypoxia-inducible factor 1 α . *Molecular cell* 2010;38:864-78.
- [45] Guarani V, Deflorian G, Franco CA, Kruger M, Phng LK, Bentley K, et al. Acetylation-dependent regulation of endothelial Notch signalling by the SIRT1 deacetylase. *Nature* 2011;473:234-8.
- [46] Herrera JE, Schiltz RL, Bustin M. The accessibility of histone H3 tails in chromatin modulates their acetylation by P300/CBP-associated factor. *J Biol Chem* 2000;275:12994-9.
- [47] Deng P, Chen QM, Hong C, Wang CY. Histone methyltransferases and demethylases: regulators in balancing osteogenic and adipogenic differentiation of mesenchymal stem cells. *International journal of oral science* 2015;7:197-204.
- [48] Rosen CJ, Buxsein ML. Mechanisms of disease: is osteoporosis the obesity of bone? *Nat Clin Pract Rheumatol* 2006;2:35-43.
- [49] Rodriguez JP, Astudillo P, Rios S, Pino AM. Involvement of adipogenic potential of human bone marrow mesenchymal stem cells (MSCs) in osteoporosis. *Curr Stem Cell Res Ther* 2008;3:208-18.

Figure legends

Fig. 1 PCAF expression is increased by osteogenic induction through Smad in MSCs

(A-C) MSCs were treated with osteogenic media for 0 day, 3 days, 7days, and 14 days, then the mRNA expression of *RUNX2* (A), *GCN5* (B), and *PCAF* (C) was assessed by RT-qPCR. (D) Immunoblotting was performed to determine the expression of GCN5 and PCAF in MSCs at 14 days after osteogenic induction. (E) The knockdown of SMAD1 by shRNA. SMAD1 expression was examined by western blot analysis. (F) The knockdown of *SMAD1* inhibited *PCAF* expression. *PCAF* mRNA was detected by RT-qPCR. (G) The knockdown of *SMAD1* inhibited *PCAF* expression, but not *GCN5* expression, as determined by western blotting. (H) The knockdown of *SMAD4* by shRNA. SMAD4 expression was examined by western blot analysis. (I) The knockdown of *SMAD4* inhibited *PCAF* expression. *PCAF* mRNA was detected by RT-qPCR. All data are shown as mean \pm SD, n = 3. ***P* < 0.01 and ****P* < 0.001. pm: proliferation media; om: osteogenic media.

Fig. 2 Knockdown of *PCAF* inhibits osteogenic differentiation *in vitro*

(A) Knockdown of *PCAF* was validated by western blotting. (B-C) *PCAF* knockdown decreased ALP activity in MSCs. Control or *PCAF* knockdown MSCs were treated with proliferation or osteogenic media for 7 days for ALP staining (B), and cellular extracts were prepared to quantify ALP activity (C). (D-E) Knockdown of *PCAF* inhibited mineralization of MSCs. Cells with or without *PCAF* knockdown were treated with proliferation or osteogenic media for 14 days, and then calcium deposition was observed using Alizarin Red S staining (D) and quantified (E). Knockdown of *PCAF* inhibited the expression of *BGLAP* (F), *SPPI* (G), and *ALP* (H) in MSCs, as determined by RT-qPCR. All data are shown as mean \pm SD, n = 3. *** P < 0.001. pm: proliferation media; om: osteogenic media.

Fig. 3 The acetyltransferase activity of *PCAF* is indispensable for the regulation of osteogenic differentiation

(A) Rescue of WT or mutant *PCAF* cell line was validated by western blotting. (B-C) Overexpression of WT *PCAF* increased ALP activity of MSCs. Control, WT or mutant *PCAF* rescue cells were treated with proliferation or osteogenic media for 7 days for ALP staining (B), and cellular extracts were prepared to quantify ALP activity (C). (D-E) Overexpression of WT *PCAF* promoted mineralization in MSCs. Cells with WT or mutant *PCAF* overexpression were treated with proliferation or osteogenic media for 14 days, and then calcium deposition was observed using Alizarin Red S staining (D) and quantified (E). Overexpression of WT *PCAF*

promoted expression of *BGLAP* (F), *RUNX2* (G), and *SPP1* (H) in MSCs, as determined by RT-qPCR. All data are shown as mean \pm SD, n = 3. ** P < 0.01 and *** P < 0.001. pm: proliferation media; om: osteogenic media.

Fig. 4 PCAF is required for MSC-mediated bone formation *in vivo*

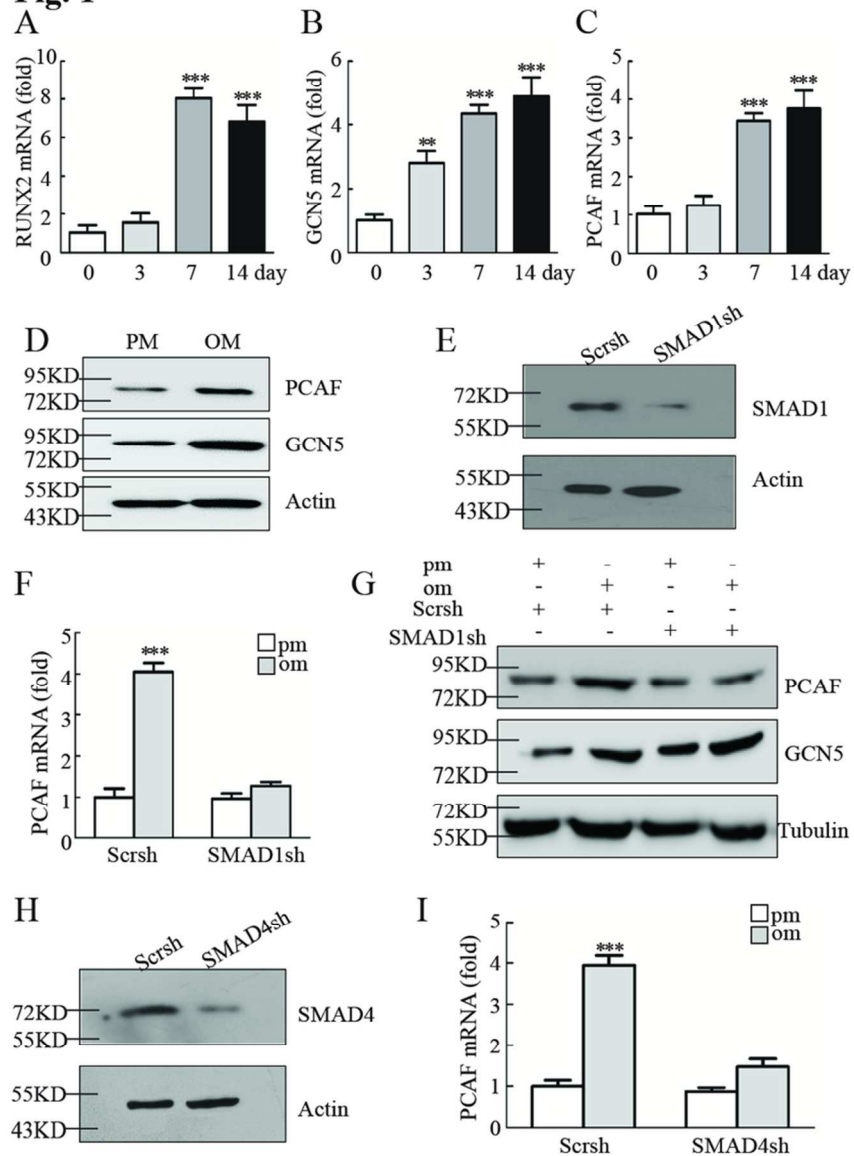
(A) Knockdown of *PCAF* reduced MSC-mediated bone formation *in vivo*, as determined by H&E staining of histological sections from implanted MSC-scaffold hybrids. Scale bar represents 100 μ m. (B) Quantitative measurements of bone-like tissues demonstrated that, at 6 weeks after implantation, the area of bone formation was significantly decreased in *PCAF* knockdown cells compared with control cells. (C) Masson's trichrome staining of histological sections from implanted MSC-scaffold hybrids. Scale bar represents 100 μ m. (D) Knockdown of *PCAF* promoted adipogenic differentiation of MSCs by oil red staining. All data are shown as the mean \pm SD, n = 3. ** P < 0.01 and *** P < 0.001.

Fig. 5 PCAF acetylates histone H3K9 at promoters of BMP pathway genes

(A-D) Endogenous PCAF is recruited to the promoters of *BMP2* (A), *BMP4* (B), *BMPR1B* (C), and *RUNX2* (D). (E-H) CHIP analysis detected H3K9 acetylation at the promoters of *BMP2* (E), *BMP4* (F), *BMPR1B* (G), and *RUNX2* (H) in WT and *PCAF* knockdown MSCs. Antibodies to acetylated H3K9 (AcH3K9) and to H3 were used, and acetylated H3K9 levels are shown relative to total H3 levels. All data are shown as mean \pm SD, n = 3. ** P < 0.01 and *** P < 0.001.

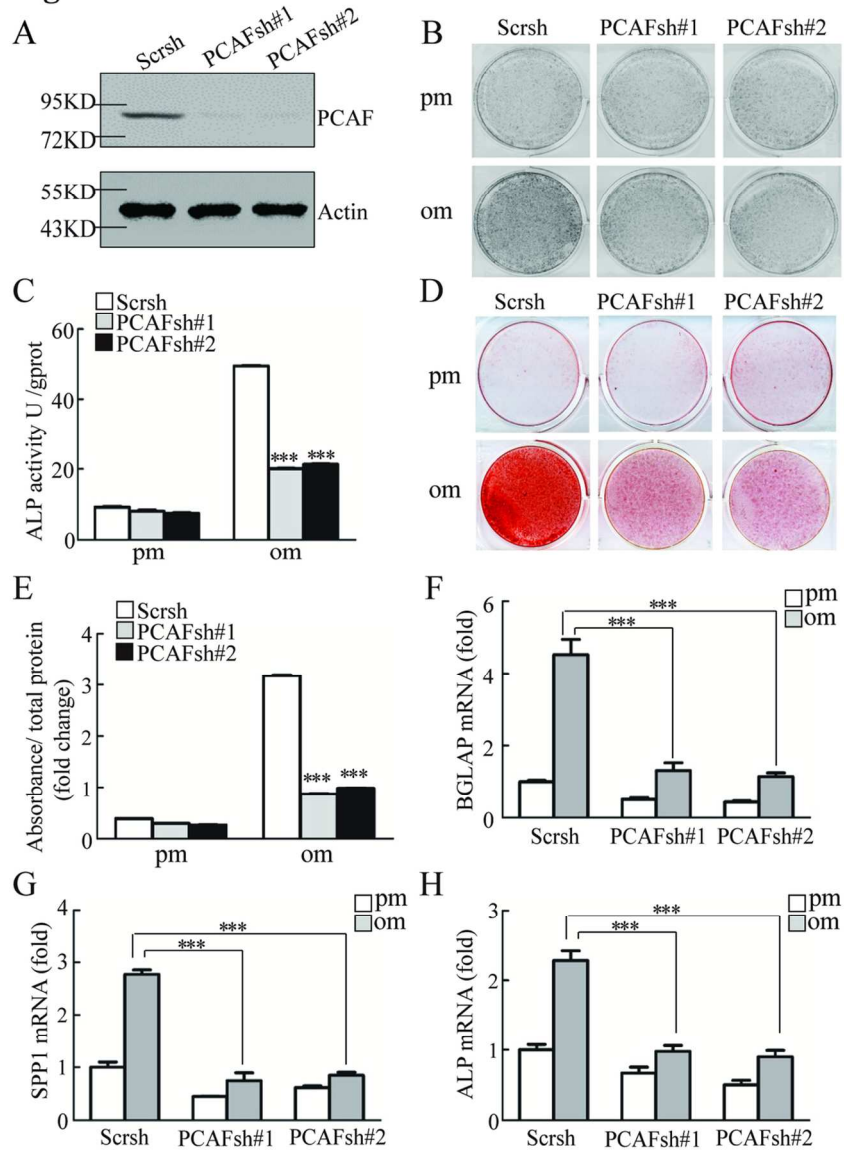
Fig. 6 PCAF are decreased in bone sections of osteoporotic mice

(A) Representative micro CT image and H&E staining of bone loss in OVX mice. Scale bar for micro CT and H&E represents 1 mm and 20 μm , respectively. (B) Trabecular number was reduced in OVX mice. (C) Bone volume was reduced in OVX mice. (D) Histology and immunofluorescence of sections from OVX mice showed decreased PCAF expression compared with sham mice. Scale bar represents 50 μm . (E) Quantification of normalized PCAF signals in (D). (F) Representative micro CT image and H&E staining of bone loss in 2-month-old mice and 16-month-old mice. Scale bar for micro CT and H&E represents 1mm and 20 μm , respectively. (G-H) Trabecular number (G), and bone volume fraction (H) were detected in 2-month-old mice and 16-month-old mice. (I) Immunofluorescence staining of PCAF in bone tissues of 2-month-old mice, and 16-month-old mice. Scale bar represents 50 μm . (J) Quantification of normalized PCAF signals in (I). All data are shown as mean \pm SD, $n=3$. $*P < 0.05$, $**P < 0.01$, and $***P < 0.001$.

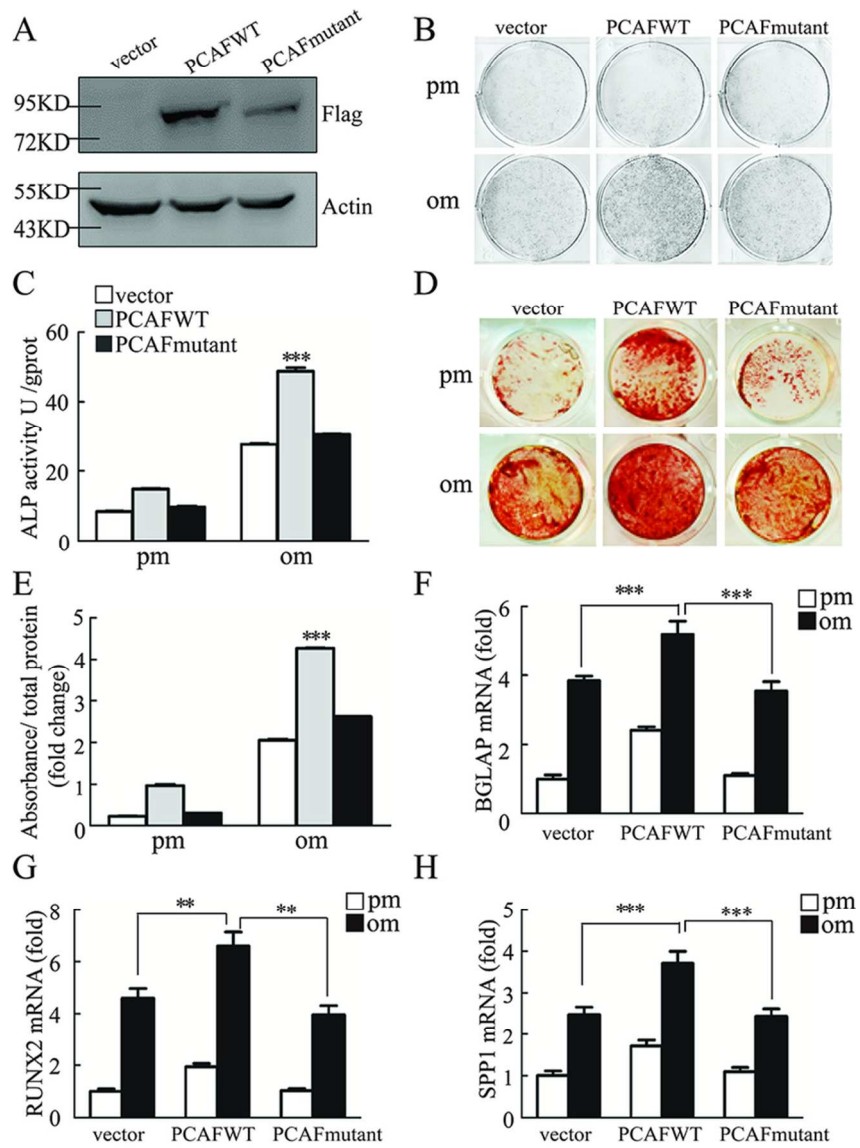
Fig. 1

35x49mm (600 x 600 DPI)

Fig. 2

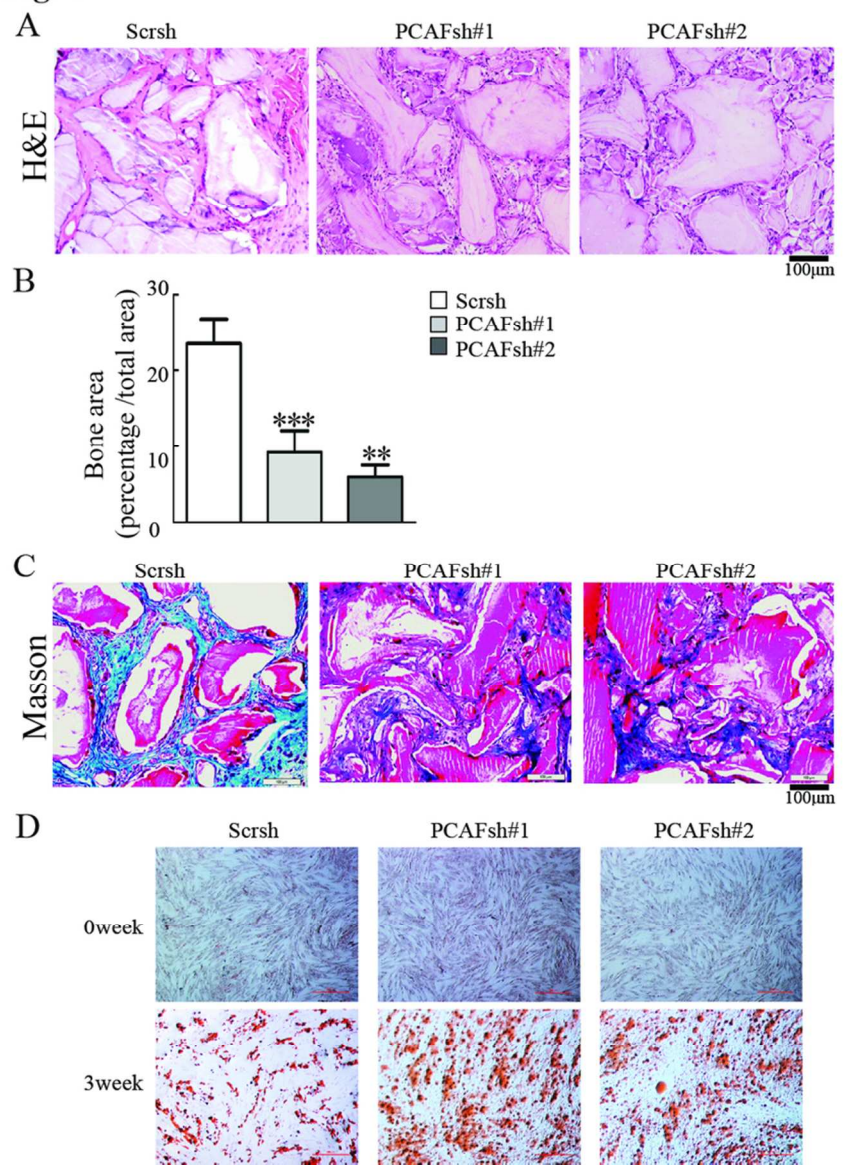


49x70mm (600 x 600 DPI)

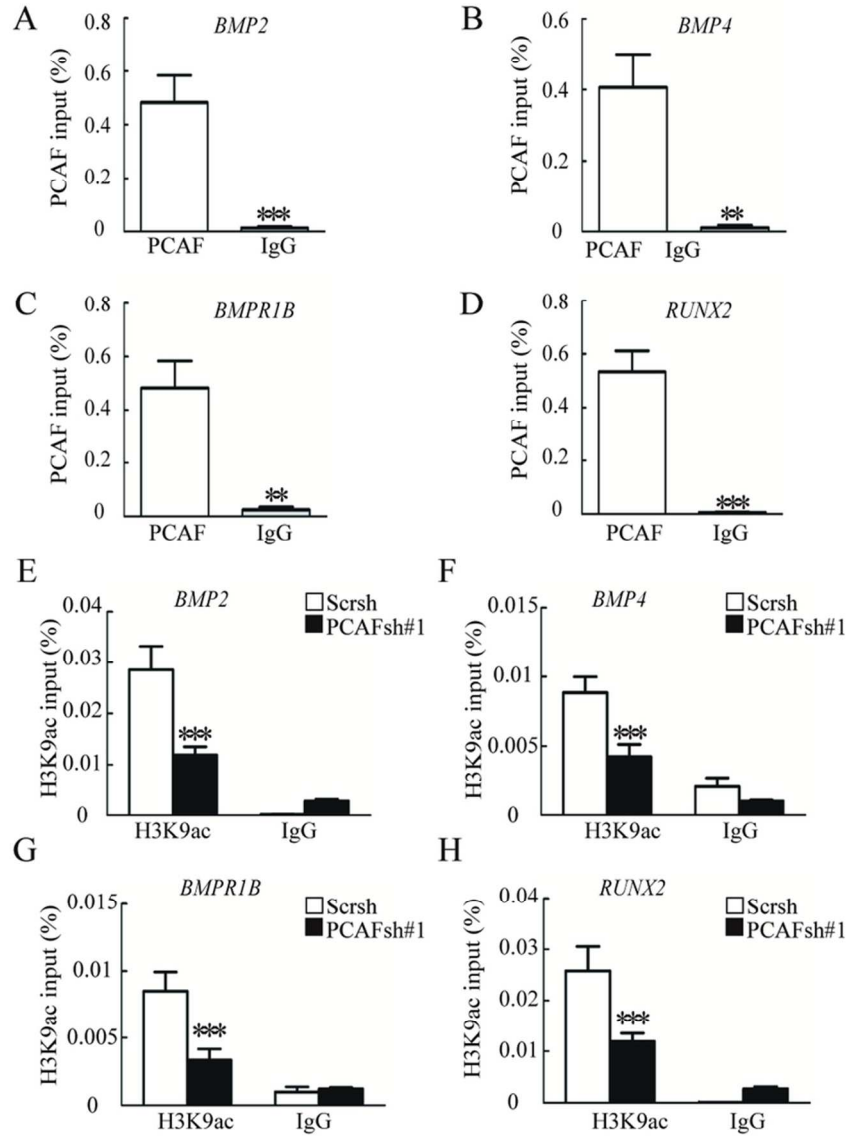
Fig. 3

35x50mm (600 x 600 DPI)

Fig. 4

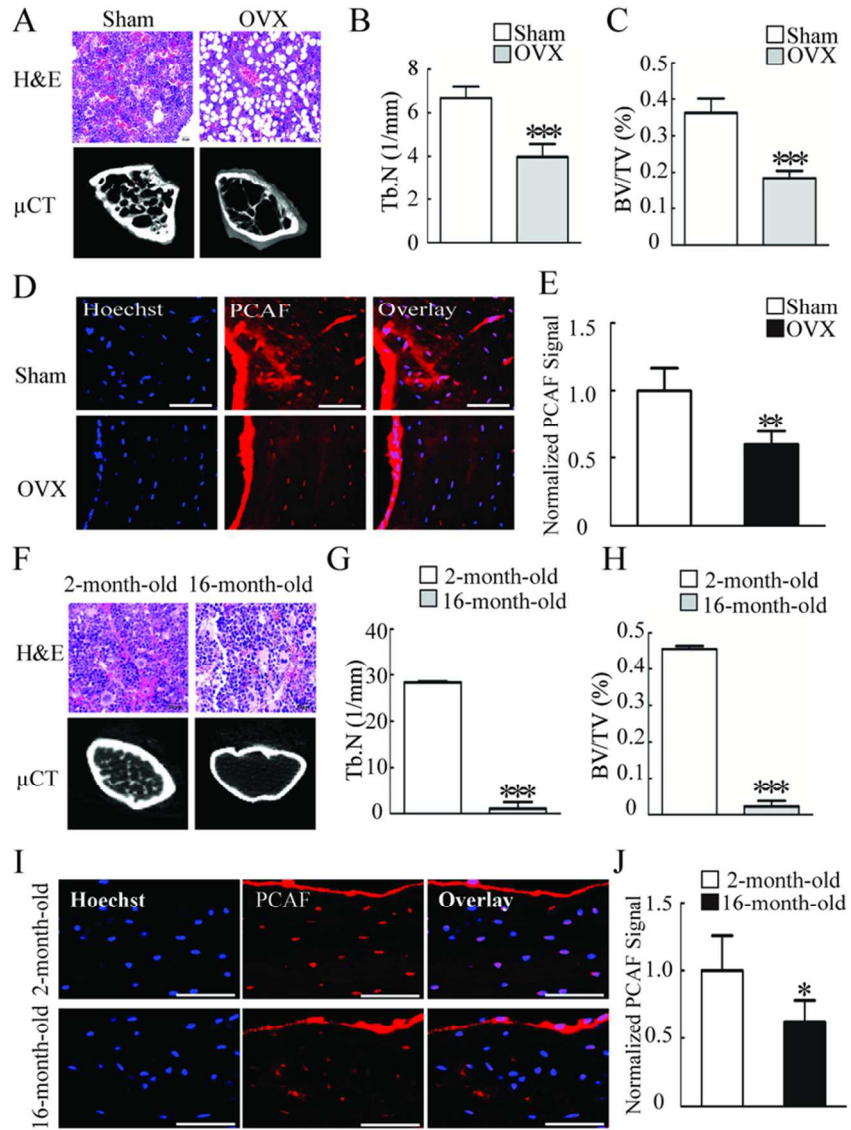


35x49mm (600 x 600 DPI)

Fig. 5

34x49mm (600 x 600 DPI)

Fig. 6



34x49mm (600 x 600 DPI)

Supplemental Information

Supplemental Fig. 1

MSCs were treated with proliferation or osteogenic media for 14 days, and then calcium deposition was observed using Alizarin Red S staining (A) and quantified (B). (C) The mRNA expression of *PCAF* and *GCN5* was assessed by RT-qPCR. (D-E) MSCs were treated with proliferation media, or osteogenic media for 7 days, or osteogenic media for 7 days in the presence of BMP2 (200ng/ml), and then *PCAF* (D) and *GCN5* (E) mRNA expression was observed using RT-qPCR analysis. (F) The knockdown efficiency of *SMAD1* in MSCs was validated by fluorescence microscopy. A1, bright field of ScrsH cells; A2, RFP-ScrsH positive cells; A3, merge of bright field and RFP-positive cells. B1, bright field of *SMAD1* sh cells; B2, RFP-*SMAD1* sh positive cells; B3, merge of B1 and B2. Scale bar represents 100 μ m. (G) The knockdown of *SMAD1* played no effect on *GCN5* expression. *GCN5* mRNA was detected by RT-qPCR. (H) The knockdown efficiency of *SMAD4* in MSCs was validated by fluorescence microscopy. A1, bright field of ScrsH cells; A2, RFP-ScrsH positive cells; A3, merge of bright field and RFP-positive cells. B1, bright field of *SMAD4* sh cells; B2, RFP-*SMAD4* sh positive cells; B3, merge of B1 and B2. Scale bar represents 100 μ m. (I) The knockdown of *SMAD4* played no effect on *GCN5* expression. *GCN5* mRNA was detected by RT-qPCR. All data are shown as the mean \pm SD, n = 3. ***P* < 0.01 and ****P* < 0.001; pm: proliferation media; om: osteogenic media.

Supplemental Fig. 2

(A) The knockdown efficiency of *PCAF* in MSCs was validated by fluorescence microscopy. A1, bright field of ScrsH cells; A2, RFP-ScrsH positive cells; A3, merge of bright field and RFP-positive cells. B1, bright field of *PCAF* sh#1 cells; B2, RFP-*PCAF* sh#1 positive cells; B3, merge of B1 and B2. C1, bright field of *PCAF* sh#2 cells; C2, RFP-*PCAF* sh#2 positive cells; C3, merge of C1 and C2. Scale bar represents 100 μm . (B) MSCs were treated with osteogenic media for 0 day, 4 days, 7 days, 10 days, 12 days, and 14 days, then the cellular extracts were prepared to quantify ALP activity. (C) Knockdown of *PCAF* inhibited the expression of *RUNX2* in MSCs, as determined by RT-qPCR. All data are shown as mean \pm SD, $n = 3$. $**P < 0.01$, and $***P < 0.001$. pm: proliferation media; om: osteogenic media.

Supplemental Fig. 3

(A) Rescue of WT or mutant *PCAF* cell line, as validated by fluorescence microscopy. A1, bright field of vector-transfection in RFP- *PCAF* sh cells; A2, RFP-*PCAF* sh positive cells with vector transfection; A3, merge of A1 and A2. B1, bright field of flag-*PCAF* (WT) infection in *PCAF* sh cells; B2, RFP-*PCAF* sh/ flag-*PCAF* (WT) positive cells; B3, merge of B1 and B2. C1, bright field of flag-*PCAF* mutant infection in *PCAF* sh cells; C2, RFP-*PCAF* sh/ flag-*PCAF* mutant positive cells; C3, merge of C1 and C2. Scale bar represents 100 μm . (B) Overexpression of WT *PCAF* promoted the expression of *ALP* in MSCs, as determined by RT-qPCR. All data are shown as mean \pm SD, $n = 3$. $***P < 0.001$. pm: proliferation media; om: osteogenic

media.

Supplemental Fig. 4

(A) Knockdown of *PCAF* reduced MSC-mediated bone formation in vivo, as determined by H&E staining of histological sections from implanted *PCAF* sh MSC-scaffold hybrids. Scale bar represents 50 μ m. (B) Masson's trichrome staining of histological sections from implanted ScrsH and *PCAF* sh MSC-scaffold hybrids. Scale bar represents 50 μ m. (C) Knockdown of *PCAF* increased *PPAR- γ* expression in MSCs as determined by RT-qPCR. All data are shown as mean \pm SD, n = 3. ****P* < 0.001.

Supplemental Fig. 5

(A) Knockdown of *PCAF* downregulated *BMP2*, *BMP4*, *BMPR1B*, and *RUNX2* expression in MSCs, as determined by RT-qPCR. (B) WT but not mutant *PCAF* promoted *BMP2*, *BMP4*, and *RUNX2* expression in MSCs as determined by RT-qPCR. (C-F) Knock-down of *PCAF* reduced *PCAF* binding to the promoters of *BMP2* (C), *BMP4* (D), *BMPR1B* (E), and *RUNX2* (F) in MSCs. The promoters of *BMP2*, *BMP4*, *BMPR1B*, and *RUNX2* were ChIP-ed with anti-*PCAF* antibodies or IgG control. All data are shown as mean \pm SD, n=3. ***P* < 0.01, and ****P* < 0.001.

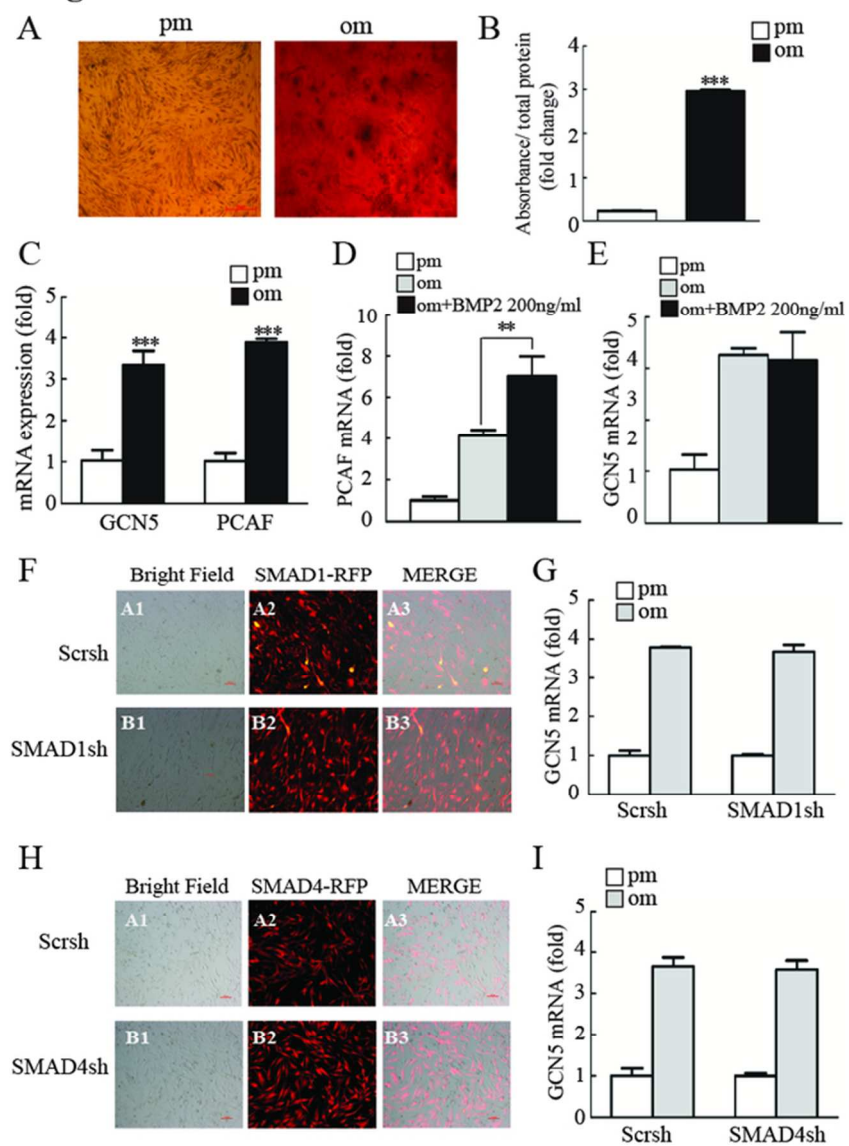
Supplemental Fig. 6

Control or *PCAF* knockdown cells, or *PCAF* knockdown cells in the presence of

BMP2 were treated with proliferation or osteogenic media for 7 days for ALP staining (A), and cellular extracts were prepared to quantify ALP activity (B). (C) Overexpression of Flag-PCAF in control and *SMAD1*-knockdown hASCs. (D) *SMAD1* knockdown diminishes the effect of PCAF on *RUNX2* expression, as determined by RT-qPCR analysis. All data are shown as mean \pm SD, n=3. *** $P < 0.001$.

Supplemental Fig. 7

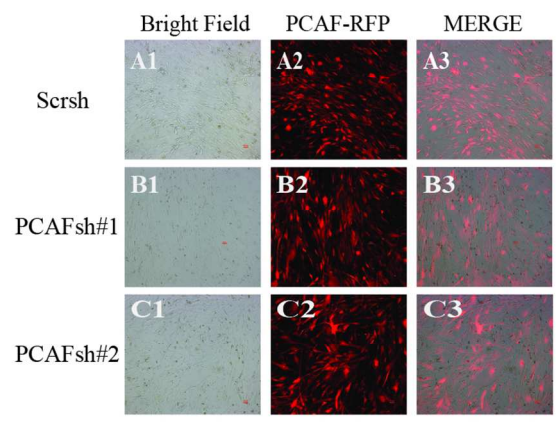
(A-B) Trabecular separation (A) and thickness (B) were detected in both sham and OVX mice. (C-D) Trabecular separation (C) and thickness (D) were detected in 2-month-old mice and 16-month-old mice. (E) Nestin positive cells in bone marrow of sham mice and OVX mice. (F) Nestin positive cells in bone marrow of 2-month-old mice and 16-month-old mice. (G) Expression of *Pcaf* was reduced in MSCs from OVX-ed mice compared with sham mice. (H) Expression of *Pcaf* was reduced in MSCs from aged mice. All data are shown as mean \pm SD, n=3. * $P < 0.05$ and ** $P < 0.01$.

SFig. 1

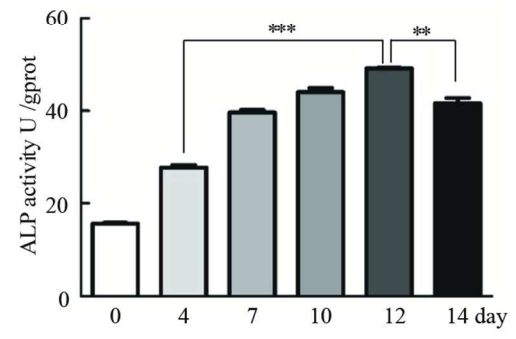
28x39mm (600 x 600 DPI)

SFig. 2

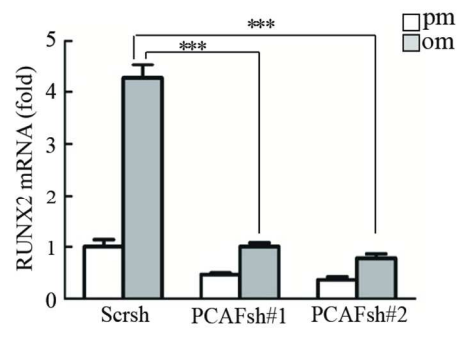
A



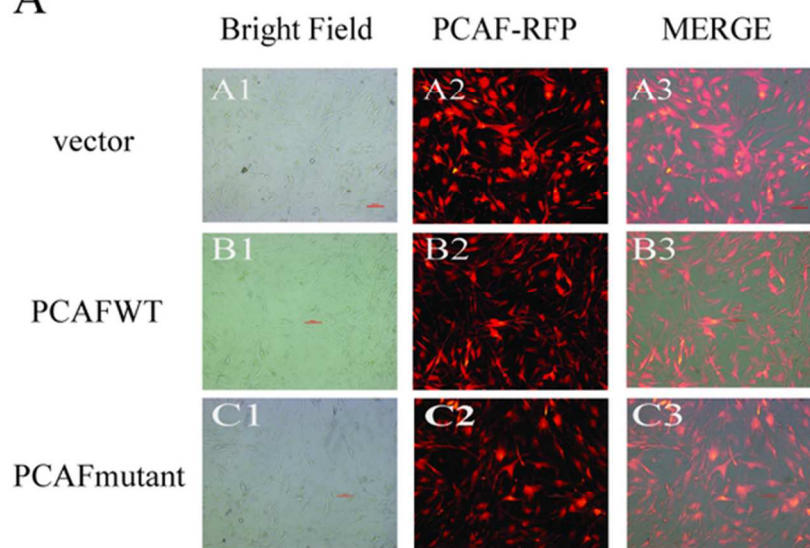
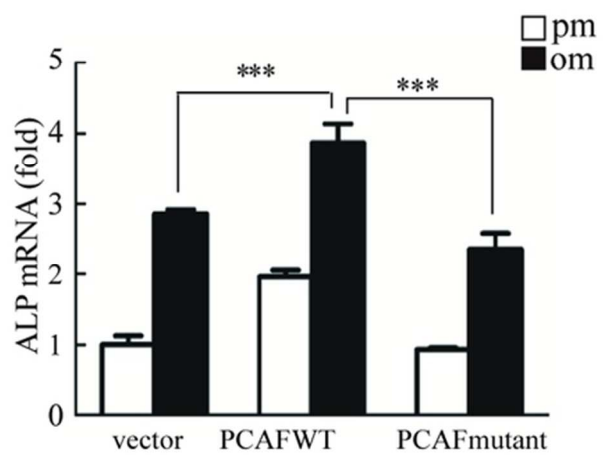
B



C

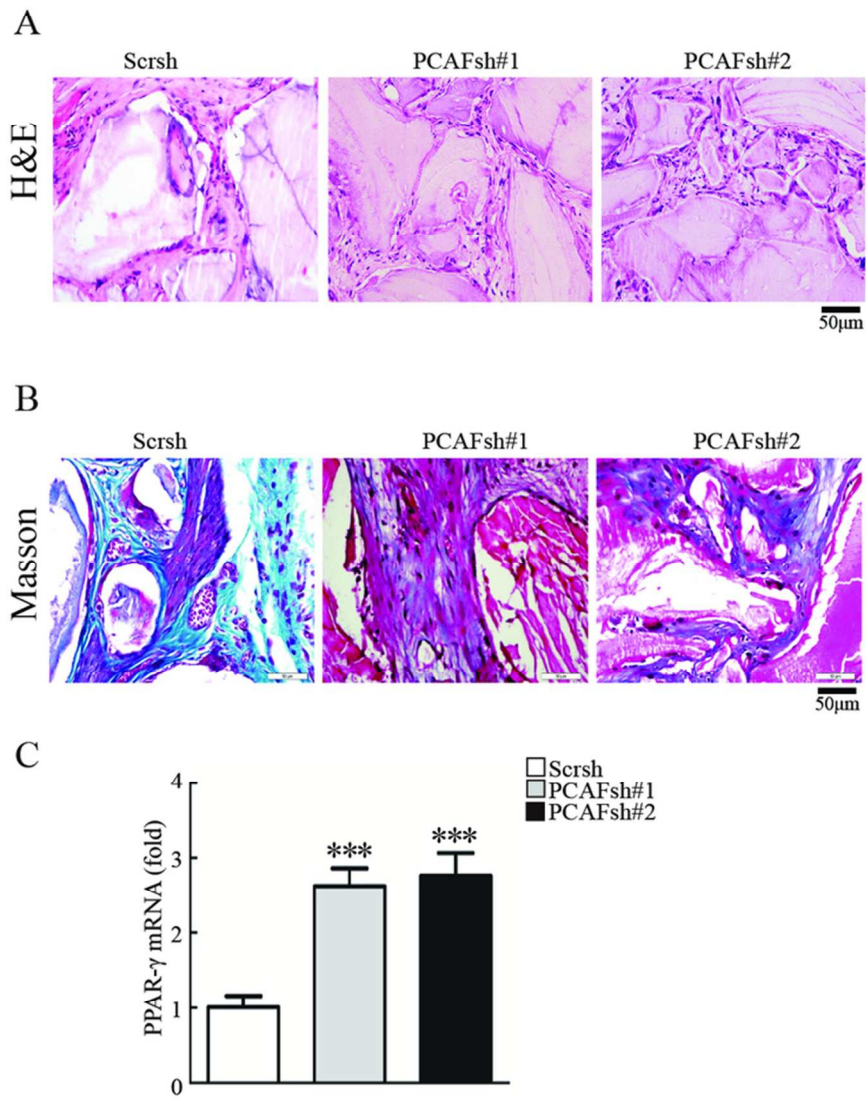


41x69mm (600 x 600 DPI)

SFig. 3**A****B**

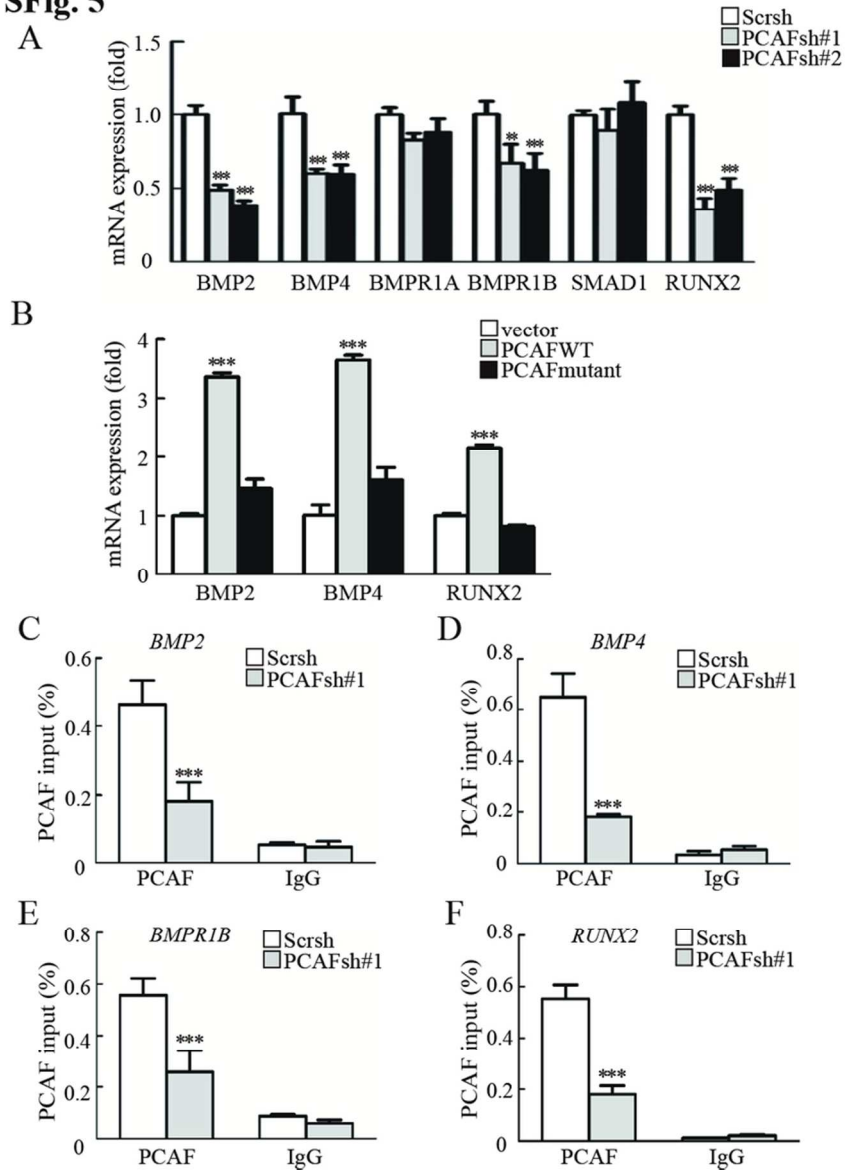
29x36mm (600 x 600 DPI)

SFig. 4



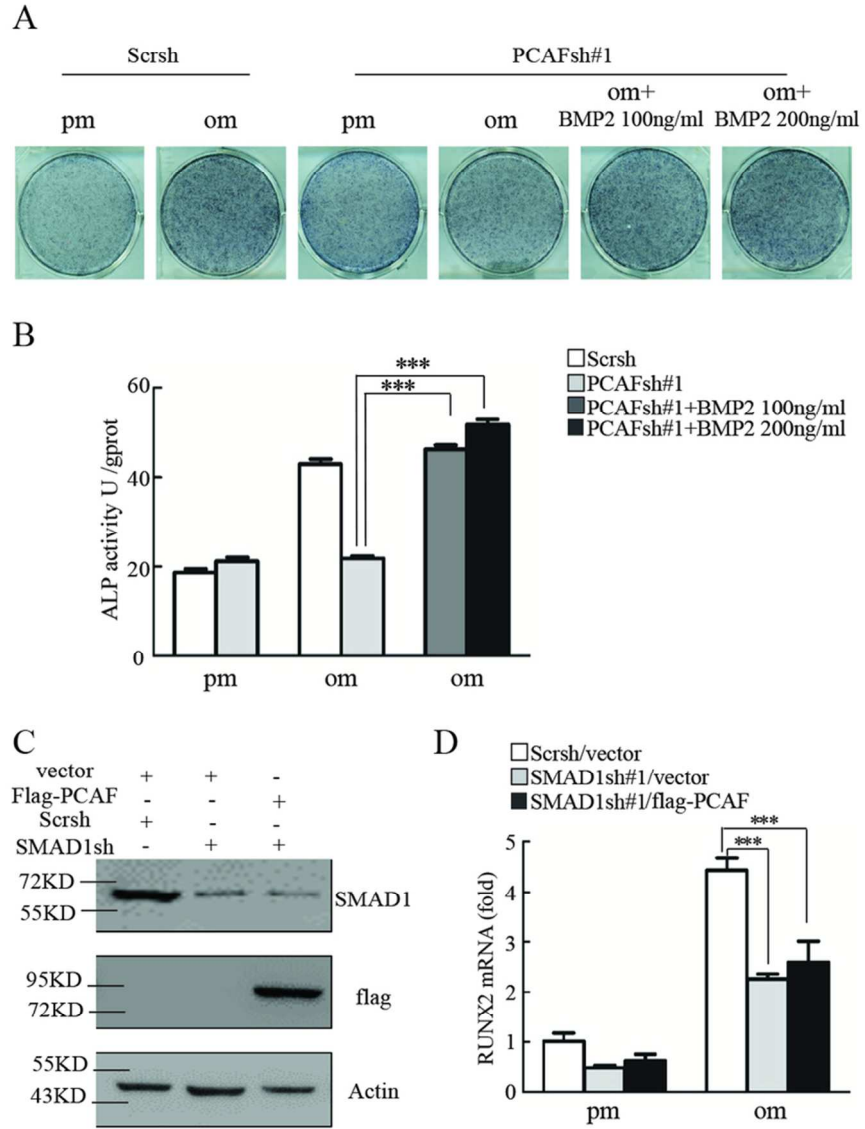
32x43mm (600 x 600 DPI)

SFig. 5



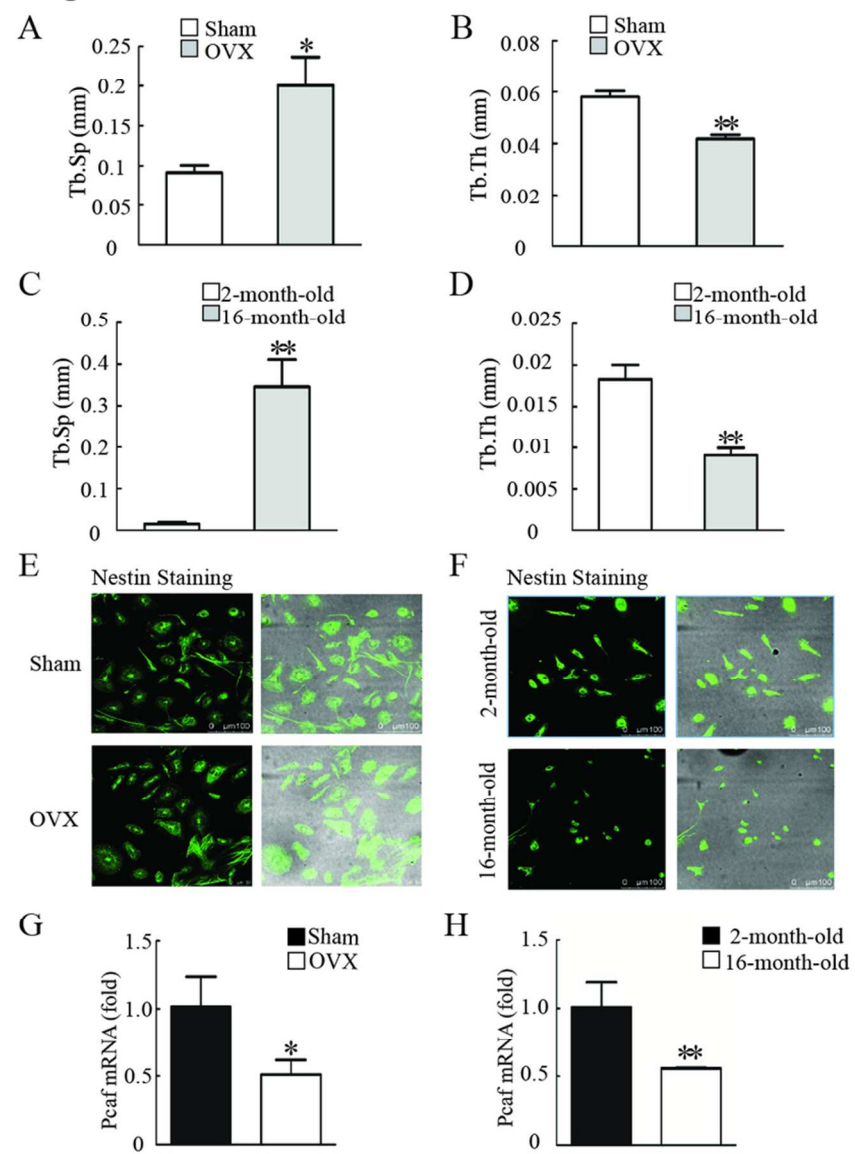
35x49mm (600 x 600 DPI)

SFig. 6

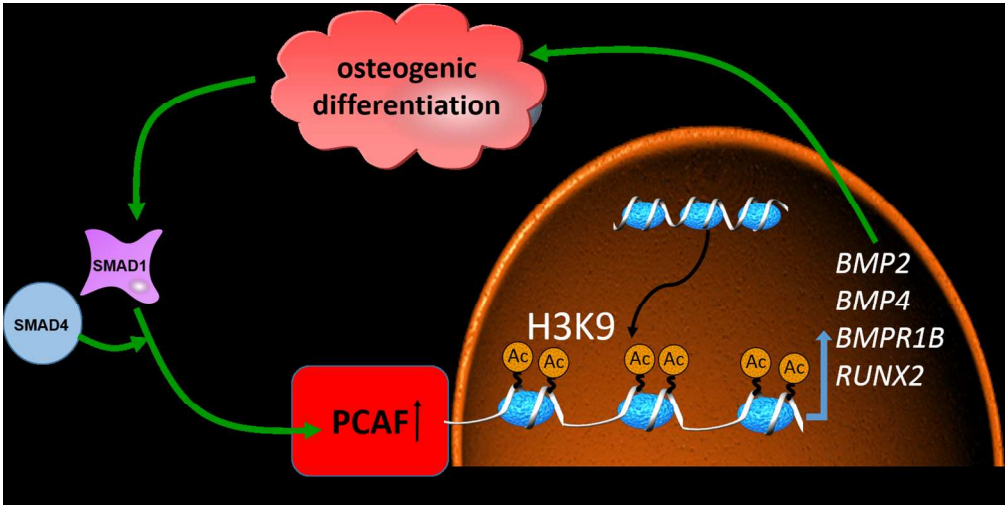


34x48mm (600 x 600 DPI)

SFig. 7



35x49mm (600 x 600 DPI)



271x135mm (150 x 150 DPI)

Osteogenic differentiation induced PCAF expression through SMADs; PCAF promoted activation of BMP2, BMP4, BMPR1B and RUNX2 by increasing H3K9ac, which led to osteogenic differentiation.